Scripta Materialia 125 (2016) 44–48

Contents lists available at ScienceDirect

Scripta Materialia

journal homepage: www.elsevier.com/locate/scriptamat

Regular Article

In-situ transmission electron microscopy investigation of the deformation behavior of spinodal nanostructured δ-ferrite in a duplex stainless steel

Yi-Chieh Hsieh [a], Ling Zhang [b], Tsai-Fu Chung [a], Yu-Ting Tsai [a], Jer-Ren Yang [a,*], Takahito Ohmura [c], Takuya Suzuki [c]

[a] Department of Materials Science and Engineering, National Taiwan University, Taipei 10617, Taiwan (ROC)
[b] College of Materials Science and Engineering, Chongqing University, Shazhengjie 174, Chongqing 400045, China
[c] National Institute for Materials Science, 1-2-1 Sengen, Tsukuba, Ibaraki 305-0047, Japan

ARTICLE INFO

Article history:
Received 14 April 2016
Received in revised form 25 June 2016
Accepted 28 June 2016
Available online xxxx

Keywords:
In-situ compression
Duplex stainless steel
Scanning/transmission electron microscopy (STEM)
Spinodal structure
Dislocation

ABSTRACT

In-situ compression tests in a transmission electron microscope were carried out to investigate the deformation behavior of δ-ferrite nanopillars of a duplex stainless steel. The δ-ferrite with a spinodal nanostructure, which formed due to aging at 475 °C for 64 h, obviously suppressed the progress of serrated yielding (a series of short strain bursts) relative to that without the spinodal nanostructure. The results revealed that during compression deformation, the spinodal nanostructure confined the movement of dislocations (leading to a significant increase in dislocation density), causing a notable strengthening effect, and also kept the slip band morphology planar.

Duplex stainless steels have been increasingly used for construction in the chemical and marine industries due to their excellent combination of mechanical properties and corrosion resistance [1–4]. The superior properties of duplex stainless steels come primarily from their approximately equivalent amounts of austenite (γ) and δ-ferrite [5]. The previous work [6] has demonstrated that after isothermal treatment in the range of 400 to 500 °C, the δ-ferrite of a 2205 duplex stainless steel becomes hard and brittle, a phenomenon known as "475 °C embrittlement". This phenomenon is well recognized to be associated with the decomposition of δ-ferrite into an iron-rich BCC phase (α) and a chromium-enriched BCC phase (α′) by spinodal decomposition [6–9]. High-resolution transmission electron microscopy and atom probe microscopy have been used to observe the spinodal structure of a duplex stainless steel [6,10], which was revealed to be a nanometer-scaled modulated structure with a complex interconnected network. It has been speculated that the interaction between dislocations and the internal coherency stress field, which is due to the periodic variation of lattice parameter in modulated spinodal structure, results in a remarkable hardening effect [11,12]. On basis of this concept, Cahn [11] first introduced a model to deal with the force on a single dislocation (pure edge or pure screw) as a function of the amplitude and the wavelength of composition modulation. Later, Kato [12] further considered the effect of periodic variation of elastic modulus and proposed a modified model to calculate the magnitude of incremental yield stress in BCC spinodal alloys, where the macroscopic yielding was assumed to be controlled by the motion of the mixed dislocation. Those models have improved the understanding of the mechanism responsible for the spinodal hardening. However, the related in-situ TEM work to reveal the interaction between dislocations and the spinodal nanostructure has not yet been reported. In the previous works [6,13–16], it has been generally recognized that the locking of dislocations by the modulated spinodal structure leads to severe embrittlement, although there is no direct TEM evidence. Clearly, it needs more work to explore the complex slip geometry in BCC spinodal alloys.

In previous works [17–23], in-situ mechanical testing with transmission electron microscopy can be used to explore the fundamental mechanisms of plastic deformation in BCC and FCC metals. Thereby, the effects of pre-existing defects (dislocations and clusters of solute) on the strength and deformation behavior of nanopillars have been investigated to elucidate the basic relationship between defects and mechanical properties. The purpose of this work was to investigate the interaction between dislocations and the spinodal nanostructure during the course of the deformation of unaged and aged δ-ferrite nanopillars (the former without, and the latter with, the spinodal nanostructure) manufactured from a 2205 duplex stainless steel. Using in-situ

* Corresponding author.
E-mail address: jryang@ntu.edu.tw (J.-R. Yang).

http://dx.doi.org/10.1016/j.scriptamat.2016.06.047
1359-6462/

nanoindentation coupled with transmission electron microscopy, the detailed dislocation characteristics and movements have been recorded and analyzed to clarify the effect of the spinodal structure on the deformation behavior of δ-ferrite nanopillars.

The chemical composition of the wrought 2205 duplex steel studied was Fe-22.62Cr-5.12Ni-3.24Mo-1.47Mn-0.38Si-0.02C (wt.%). The as-received 2205 duplex stainless steel rods were produced by Gloria Material Technology Corporation, Taiwan, through the 4-folded forging of a cast slab at 1160–1180 °C, followed by annealing of the steel at 1050 °C for 30 min and water quenching. The annealed steel had a dual-phase structure (with 45 δ-ferrite and 55 austenite, vol.%) without other secondary phases. The composition of δ-ferrite was determined by EMPA to be Fe-23.8Cr-3.86Ni-3.92Mo-1.35Mn-0.44Si (wt.%). Two specimens with dimensions of 5 mm × 5 mm × 3 mm were machined from the two steel rods, respectively. One of the rods was not heat treated by aging and the other was aged at 475 °C for 64 h. These two specimens were then mechanically and chemically polished. A JEOL JBM-7000F with EDAX EBSD (electron backscatter diffraction) was employed to determine the chosen grain for a specific orientation. Through the pole figures, the δ-ferrite single grain (sectioning the 001 pole for the in-situ compression direction and the 100 pole for the observation direction) was machined into 20 μm × 15 μm × 3 μm thin platelets with a focused ion beam instrument (JEOL JEM-4000 FIB). Carbon was deposited on the polished platelets before the preparation of the nanopillars to reduce damage from the incident Ga^{+} ions. Finally, nanopillars of ~600 nm in length, ~300 nm in width, and ~100 nm in thickness were fabricated from the edges of the platelets with a focused ion beam instrument (JEOL JEM-9320 FIB). An illustration of the nanopillar fabrication process is provided in Supplementary Fig. 1. The pillars were compressed uniaxially along the [001] direction at room temperature in a JEOL 2010F transmission electron microscope with a Hysitron PicoIndenter installed. A diamond flat-end conical indenter with a diameter of ~2.5 μm at the free end was applied. The system was operated in the displacement-control compression mode with a maximum strain of 0.3–0.6 and a displacement rate of 1 nm s^{-1}, and the deformation processes were recorded as videos. Conventional TEM and scanning TEM (STEM) modes were also used to observe the dislocation structures during in-situ nanoindentation.

Fig. 1a presents a TEM bright field image taken from the δ/γ interface of the aged specimen. What is remarkable is the sudden change from the modulated contrast in the δ-ferrite grain to an even contrast in the austenite grain. This mottled aspect is attributed to the spinodal structure. This low-magnification TEM image presents the appearance of an orange peel spread uniformly all over the δ-ferrite grain [6]. However, the high-resolution TEM observation in Fig. 1b reveals the detailed interconnected spinodal structure, composed of 5–10 nm Fe-rich dark-image domains (α) and Cr-enriched bright-image domains (α').

Fig. 2 presents individual frames from a video of an unaged δ-ferrite nanopillar undergoing compression deformation. The video is provided in Supplementary Material I (Video 1). The corresponding strains are labeled in the bottom left corner of each image. The corresponding stress-strain curves are plotted in the upper right corner of each image. The stress-strain curve was calculated from the measured loads over the cross-sectional area of the nanopillar. As shown in Fig. 2a, the compression deformation was executed along the [001] direction of the single crystal nanopillar, and the diamond indenter moved from the bottom right corner to the upper left corner. The observation direction was close to the [100] direction under the two-beam condition g = [002] to render all dislocations in the bcc crystal visible [24]. After initial elastic deformation, the yielding took place at the stress of $\sigma \approx 0.9$ GPa (with strain, $\varepsilon \approx 0.04$) as shown in Fig. 2b, and the first small strain burst started at $\sigma \approx 1.2$ GPa (with $\varepsilon \approx 0.05$) as shown in Fig. 2c. In this small pop-in event, the stress dropped slightly during the course of compression deformation, and the nanopillar was still in contact with the diamond indenter. It should be noted that as the length of pillar was suddenly shortened, the stress relaxation was more closely related to the strain burst. This phenomenon has been recognized to be related to the dislocation avalanches (the group dislocations rapidly disappear) [20–23]; i.e., the group dislocations move a short distance of around several hundred nanometers to the surface of the nanopillar. As the compression deformation continued, the second small strain burst was triggered at $\sigma \approx 1.3$ GPa (with $\varepsilon \approx 0.07$). Fig. 2d shows the frame with the stress-strain curve for the stage just after the second small strain burst. After a series of the short strain bursts, the mobile dislocations were seriously entangled and their movement was restricted within the crystal. The plastic deformation was presumably carried out by the further dislocation activation from the possible multiple sources (e.g., Frank-Read sources) that activated the dislocations. When continued compression deformation was executed at stress of about 1.5 GPa, the large strain burst took place; the nanopillar specimen detached from the indenter completely and the stress dropped to zero. Fig. 2e shows the frame with the stress-strain curve for the stage just after the large strain burst. Such a large strain burst has been ascribed to the slip band formation with escape and annihilation of a considerable number of dislocations at the specimen surface, suddenly leading to a significant change in the length of pillar [20]. The slip band was planar in its initial forming stage, and the change in its geometry (during the further compression) would be involved with the activation and operation of numerous slip systems. The arrows and dotted lines in Fig. 2e delineate the curved slip band across the pillar edges, and the shape of

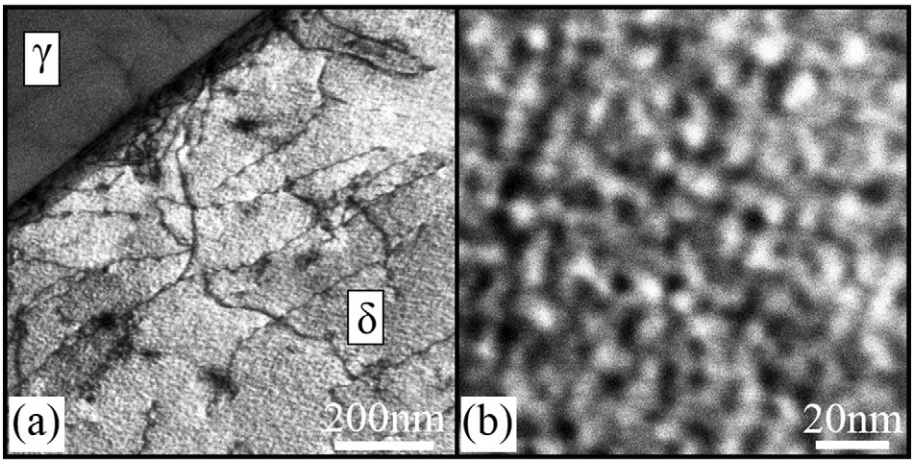

Fig. 1. TEM bright field images of the aged specimen: (a) around the δ/γ interface; (b) modulated contrast of the spinodal structure.